INIS
TRN AU7904144

AAEC/E468

AAEC/E468

AUSTRALIAN ATOMIC ENERGY COMMISSION

RESEARCH ESTABLISHMENT

LUCAS HEIGHTS

THE DETERMINATION OF TRACE QUANTITIES OF THORIUM AND URANIUM IN THICK ORE SAMPLES BY PROTON-INDUCED X-RAY EMISSION

by

D.D. COHEN*
P. DUERDEN
E. CLAYTON

*Australian Institute of Nuclear Science and Engineering

July 1979

ISBN 0 642 59673 5

AUSTRALIAN ATOMIC ENERGY COMMISSION
RESEARCH ESTABLISHMENT
LUCAS HEIGHTS

THE DETERMINATION OF TRACE QUANTITIES OF THORIUM AND URANIUM IN THICK ORE SAMPLES BY PROTON-INDUCED X-RAY EMISSION

by

D.D. COHEN*
P. DUERDEN
E. CLAYTON

ABSTRACT

Proton-induced X-ray emission (PIXE) techniques have been used to estimate the concentrations of trace quantities of thorium and uranium in powdered rock and ore samples. Standards of known concentrations were prepared in a carbon matrix and the yields from these used to determine simultaneously the concentrations of thorium and uranium in the ore samples. The experimental detection limit of the technique was found to be 3 to 4 $\mu g\ g^{-1}$ for a 100 μC irradiation. The appropriate matrix corrections for a carbon and ore matrix have been calculated for thick targets and taken into consideration.

---

*Australian Institute of Nuclear Science and Engineering

National Library of Australia card number and ISBN 0 642 59673 5

The following descriptors have been selected from the INIS Thesaurus to describe the subject content of this report for information retrieval purposes. For further details please refer to IAEA-INIS-12 (INIS: Manual for Indexing) and IAEA-INIS-13 (INIS: Thesaurus) published in Vienna by the International Atomic Energy Agency.

X-RAY EMISSION ANALYSIS; PROTON BEAMS; TRACE AMOUNTS; URANIUM; THORIUM; ORES

CONTENTS

1. INTRODUCTION

Proton-induced X-ray emission (PIXE) has been widely used for trace element analysis during recent years [Folkmann *et al.* 1974; Deconninck *et al.* 1975; Johansson & Johansson 1976; Deconninck 1977; Kaji *et al.* 1977; Mittler *et al.* 1977; Raith *et al.* 1977]. The technique has a wide range of applications including biological, archaeological and geological topics [Bearse *et al.* 1974; Walter *et al.* 1974; Nielson *et al.* 1976; Simpson & Dyson 1977; Guffey *et al.* 1978]. The method is fast, non-destructive and, for thick targets, requires only minimal target preparation. Information about many elemental concentrations can be obtained simultaneously for concentrations from 100 per cent down to several parts per million by weight ($\mu g\ g^{-1}$).

A complete PIXE system has been set up at the AAEC Research Establishment and is described in detail elsewhere [Cohen & Duerden 1979]. Concentrations of naturally occurring thorium and uranium in powdered ores have been studied over the concentration range 10 to 10 000 $\mu g\ g^{-1}$. Standards were prepared in a carbon matrix and the matrix effects for these and two known Canadian standard ores [Flanagan 1973; Abbey *et al.* 1975] were compared.

Theoretical calculations for the thick target yields for carbon and ore matrices have been calculated and compared with experimental results. Theoretical differences in the thorium and uranium Lα X-ray line yields for a carbon matrix and a typical ore matrix (silica) were of the order of 14 per cent for the AAEC detection system; the experimentally measured difference was about 11 per cent. Statistical and experimental errors were larger for very low concentrations (< 100 $\mu g\ g^{-1}$).

Throughout this report, the term, 'lower level of detection' denotes an experimentally measured value which is three standard deviations above the background. The term 'sensitivity' is the extrapolated lower limit of the experimental data.

Other techniques to measure thorium or uranium at the $\mu g\ g^{-1}$ level in a variety of matrices have been reported. Keenan [1975] used tube excited X-ray fluorescence (XRF) to determine the thorium concentrations in optical glass down to levels of 87 $\mu g\ g^{-1}$ with an error of 27 per cent. Similarly Giauque *et al.* [1977] used XRF techniques to detect thorium and uranium levels in geochemical and coal fly ash samples down to $(6 \pm 3)\ \mu g\ g^{-1}$ in their standards and $(9 \pm 6)\ \mu g\ g^{-1}$ in their fly ash; errors were quoted for the $\pm 2\sigma$ confidence interval. In three

experiments, the signal-to-noise ratio for a 100 μg g^{-1} peak in the 13 keV X-ray region was around 2:1 at best. The PIXE technique showed much lower backgrounds in this region. Runs for similar times (500 μC irradiations) gave a peak-to-background ratio of around 25:1 for a 100 μg g^{-1} peak.

Mahajan *et al.* [1977] discuss a track registration technique for the estimation of trace quantities of uranium in rock or ore samples. Samples were dissolved and then irradiated in a reactor for 7 to 8 hours at a flux of 10^{12} neutrons cm^{-2} s^{-1}. After etching in NaOH, tracks in the dielectric plastic detectors were counted and related to the uranium concentration. For known standard solutions, a lower level detection limit of 3 μg g^{-1} was quoted; however, for the powdered rock samples, this lower limit was 100 μg g^{-1}. D'Silva & Fassel [1977] have used the X-ray excited optical luminescence technique to measure uranium concentrations in ores down to 50 μg g^{-1} with a relative error at the ± 1σ level of 3.3 per cent. They quote a sensitivity of 5 μg g^{-1}.

Other more accurate methods for thorium and uranium determination are available. The isotope-dilution technique can yield accurate results for uranium and thorium to better than ± 1 per cent (3σ) of the amount present over the range 0.5 to 1000 μg g^{-1}. Delayed neutron activation for uranium and neutron activation for thorium can be used to measure concentrations of ~ 1 μg g^{-1} with 10 per cent error [Wall 1978] but the theoretically predicted detection limits for these techniques are considerably lower [Ragaini *et al.* 1976]. A major advantage of the PIXE technique over others is that the thorium and uranium concentration can be obtained simultaneously after just a few minutes' irradiation; also the use of thick targets keeps sample preparation times to a minimum.

2. THE EXPERIMENT

A schematic diagram of the experimental arrangement is shown in Figure 1. A 3 MeV Van de Graaff accelerator is used to produce 2.26 MeV protons which interact with the target to produce characteristic X-rays. The target chamber is insulated ($\gtrsim$ 70 MΩ) from the rest of the experiments and acts as a Faraday cup for charge collection and integration to give a measure of the total current hitting the target. A carbon filament for flooding insulated targets with electrons is attached to the top of the target chamber which is kept at a base pressure of 0.5 mPa. At the base of the chamber is a 25 μm beryllium window below which is the detection system.

Up to 45 pelletised ore samples were placed on a 1 m long aluminium target stick, which was moved through the incident proton beam by a computer-controlled stepping motor. Lower energy X-rays (< 10 keV) produced in the target were selectively absorbed by Perspex filters (1.5 mm thick) placed between the base of the chamber and the detector. The column of air (itself a filter for low energy X-rays) between the chamber and the top of the detector was kept at a constant length of 3 cm and the distance from the front face of the detector to the target was 15 cm.

3. THE DETECTOR

The detector is an intrinsic hyper-pure n-type silicon chip, built at the AAEC Research Establishment [Beech & Eberhardt 1973], with an active area of 50 mm^2 and a depletion thickness of 5 mm. The resolution (full width half maximum (FWHM)) is 285 eV at the Mn Kα 5.9 keV line; this rises to 313 eV at the Th Lα (~ 13 keV) line.

For the experiment, four Perspex filters (6 mm total thickness) were used to absorb the lower energy X-ray continuum and the bulk of the characteristic X-rays of the matrix (Si, K, Ca, *etc.*). The efficiency of the detection system under these conditions fitted the following empirical relationship [Cohen & Duerden 1979]:

$$\text{Eff\%} = 100 \exp\left[-AE_x^{-3}\right] \quad \text{for} \quad (10 < E_x < 20)\ \text{keV}, \qquad (1)$$

where A = (2350 ± 180) and Eff% is relative to the no filter case. From Equation (1), it can be seen that this system was 34 and 40 per cent efficient for the thorium and uranium Lα lines, respectively, relative to the no filter case. The filters not only cut the count rate into the spectrum from the unwanted low energy continuum, but also reduced the count rate, by a factor of approximately three, into the desired thorium and uranium Lα peaks. This loss of counts was not a problem; its effect on the system's sensitivity is discussed later.

4. THE ELECTRONICS

A schematic diagram of the electronic system for this experiment is shown in Figure 2. The linear signal from the detector preamplifier is shaped by an ORTEC 739 amplifier to produce a time-to-peak of 6 μs and a total base width of 60 μs. The shaped linear amplifier output is sent to an ORTEC 800 analogue-to-digital computer (ADC), set to 2048 channels,

digitised and fed into a PDP15 computer for final analysis. The busy-outs from the amplifier and the ADC are OR'd; they gate the digitised total charge pulses to produce digitised live time charge pulses which are counted in CAMAC scalars and presented to the PDP15 for manipulation. Spectra can be analysed in real time on the PDP15 or stored on disc or magnetic tape for more detailed analysis on the central computer.

The deadtime correction method has been tested to 2.5 kHz count rate and 40 per cent deadtime and found to be quite satisfactory. The pulse pair resolution of the ORTEC amplifier is ~ 500 ns, so at large count rates (> 2 kHz), sum peaks for only the largest peaks in the spectrum ($\gtrsim 10^4$ counts) can be seen. Typical count rates for our thorium/uranium analysis are 50 to 100 Hz, giving deadtimes less than 1 per cent, so pulse pileup and sum peaks can be ignored.

5. SAMPLE PREPARATION

Two types of sample were prepared:

(a) Known weights of thorium oxide and uranium oxide were added to a pure carbon matrix. These were called 'standards'.

(b) Ores and powdered rock samples of known thorium and uranium content (bulk and trace concentrations were measured elsewhere). These were called 'ores'.

To test the thoroughness of our mixing techniques for the standard samples, two methods of preparation were used:

(i) A known weight of fine powdered thorium oxide/uranium oxide was mixed with a known weight of spectroscopically pure graphite powder and shaken mechanically for 30 min. These mixtures were homogeneous down to a concentration of 250 $\mu g\ g^{-1}$.

(ii) A known weight of thorium oxide/uranium oxide was dissolved in 15 *N* HNO_3 acid and diluted to 100 mℓ. After wetting a known weight of pure graphite powder with ethyl alcohol, the required volume of thorium/uranium solution was pipetted onto the 'wet sand-like' sludge of graphite and tapped until mixing was complete. The resultant sludge was dried under arc lamps, placed in a muffle furnace at 400°C for 15 min and then shaken for 20 min. This method proved more satisfactory than direct mixing and enabled homogeneous concentrations down to

10 μg g^{-1} to be prepared.

After mixing, the powders were placed into pure (99.9 per cent) aluminium caps (13 mm diameter) and pelletised at 14 MPa for 60 s. The final pellets had flat, well-defined front faces and were a very convenient size for mounting in the long target sticks.

The powdered ore or rock samples (particle size $\lesssim$ 1 μm) were placed into the aluminium caps and pelletised. No other sample preparation was carried out for these ores.

Standard thorium/uranium and ore samples were prepared in the range 10 to 10 000 μg g^{-1}. The standard samples were good thermal and electrical conductors, enabling currents as high as 500 nA to be used for an indefinite period. This was not the case for some ore samples; currents this high made the target red hot, and target charging effects, even with electron flooding, produced such high backgrounds in the X-ray spectra that the sensitivity was severely reduced. Under these conditions, the maximum target current was limited to ~ 350 nA.

6. THORIUM/URANIUM X-RAY SPECTRA

Thorium and uranium have several characteristic X-ray lines. The K series lines appear in the 90 to 110 keV region but these were ignored since the detector has a very low photopeak efficiency. Accordingly, measurements were taken using the L series lines in the 11 to 21 keV region where the detector efficiency is high. The M series lines in the 2 to 3 keV region were completely absorbed by the four Perspex filters.

A typical PIXE spectrum for a standard 75 μg g^{-1} sample of thorium and uranium is shown in Figure 3. Seven separate L lines were resolved for both thorium and uranium. The measured intensities of these lines normalised to Lα ≡ 1 are given in Table 1. Figure 4 shows a typical spectrum for an ore sample; here, the K series lines for strontium, yttrium and zirconium are mixed with the L series lines from lead, thorium and uranium. These spectra were background and peak fitted by the techniques described in Section 7 and the thorium/uranium Lα peak areas extracted and related to the known sample concentrations.

All standard and ore sample spectra were obtained under the following run conditions:

- Proton beam energy was 2.26 MeV.
- A 2 mm diameter aperture was used for proton beam collimation 1.5 m upstream from the target.

- Each target received a total deadtime corrected charge of 500 μC. Beam currents varied between 300 and 500 nA, depending on the target.
- The electron flood was 'on' (carbon filaments red hot) for all samples. This eliminated any possible systematic current measurement errors produced by the electron flood.
- The target was at 45° to the incident proton beam and normal to the detector surface.
- Full detector sensitive area was used (50 mm^2), *i.e.* no X-ray collimation.
- Four Perspex filters (6 mm total thickness) were used to absorb the low energy X-ray continuum.

7. BACKGROUND ESTIMATION AND PEAK FITTING

As the background and peak fitting routines are to be published in detail [Clayton *et al.* forthcoming], only a summary will be given here. For the standard samples, a carbon matrix was used and a carbon blank sample background was normalised in the 20 to 22 keV spectrum region to the standard sample background for this region. Figure 5 shows a typical carbon blank background for the four-filter case and the zero-filter case. Slight iron, copper and zinc impurities (equivalent to about 50 μg g^{-1}) can be seen in both spectra. The background in the 10-20 keV region, which contains the thorium/uranium L lines, is free from impurities and averages out at ~ 10 counts per channel per 500 μC or less; this is a most acceptable limit. The iron, copper and zinc impurities have three possible sources: scattering by the target of X-rays produced at the proton-defining brass aperture 1.5 mm upstream from the target; impurities in the Al target holder excited by the beam halo; or impurities in the target carbon matrix itself. The first possibility is thought to be the most probable cause.

Although not in a carbon matrix, the background spectra for the ores were similar in shape to those of the standard samples for the energy region 5 to 25 keV; consequently, the normalised carbon blank background was also used for the ore samples. The background plus peak spectrum was fitted, channel by channel, to a function of the form:

$$Y(E) = \sum_{jk} R_{jk} G_{jk} + BKG(E) \quad , \qquad (2)$$

where R_{jk} is a matrix of relative peak intensities at X-ray energies E_{jk} for element j and BKG(E) is the background as a function of energy (channel number).

$$G_{jk} = \exp - \frac{(E-\mu)^2}{2\sigma^2} \tag{3}$$

is a Gaussian peak shape, where

$$\begin{aligned} \mu &= p_1 + p_2 E_{jk} \\ \sigma &= p_3 + p_4 E_{jk} \end{aligned} \quad . \tag{4}$$

Gaussian line shapes were used to fit the characteristic X-ray peaks. However, large peaks ($> 10^4$ counts) are asymmetric with low energy tails, as shown in Figure 6. To fit these asymmetric peaks, exponential tails and step functions of the following forms were used:

$$G_{jk} = G+T+S \quad , \tag{5}$$

where $T = p_5 \exp(p_6(E-\mu)) \quad E < \mu$, tail function (6)

$$S = p_7 \operatorname{erfc} \frac{(E-\mu)}{\sigma\sqrt{2}} \quad , \qquad \text{step function} \tag{7}$$

The parameters p_1 to p_7 were varied in a least squares fitting program until χ^2, defined by Equation (8), changed by less than 1 per cent.

$$\chi^2 = \frac{1}{N-P} \sum_i \frac{(Y_i - Y_{expt})^2}{\sigma^2_{expt}} \quad , \tag{8}$$

where P is the number of parameters, N is the number of channels used for fitting, and Y_i, Y_{expt} are the fitted and experimental yields, respectively, for channel i and have a standard deviation σ_{expt}.

Having fitted the complete spectrum by the sum of these resolved Gaussians, and obtained fits like those shown in Figures 3 and 4 with a χ^2 goodness of fit around unity, the peak areas associated with each Gaussian, and hence each characteristic X-ray line for an element, could be extracted.

8. RESULTS AND DISCUSSION

Once the thorium/uranium Lα peak areas are known, they can be plotted against the known concentrations of thorium and uranium for both the standards and the ores (Figures 7 and 8). Good linearity over four

decades of concentration (1 to 10^4 μg g^{-1}) was obtained for both the thorium and uranium results. The standards (X) and the ores (O), together with their least squares fitted lines, are shown separately on each graph. The lines of best fit have been forced to go through the origin. For the four cases:

(i) Thorium Lα in carbon matrix, counts/500 μC = 14.8 x concentration (μg g^{-1}).

(ii) Thorium Lα in ore matrix, counts/500 μC = 16.4 x concentration (μg g^{-1}).

(iii) Uranium Lα in carbon matrix, counts/500 μC = 12.9 x concentration (μg g^{-1}).

(iv) Uranium Lα in ore matrix, counts/500 μC = 14.2 x concentration (μg g^{-1}).

The yields for cases (i) to (iv) have been obtained for the four-filter case.

In Figure 3, the background in the 13 keV energy region is ~ 4 counts per channel, giving a total background area under the thorium/uranium Lα peak of ~ 150 counts/500 μC. For a 3σ confidence limit, where σ is equal to $\sqrt{\text{background}}$, this gives a lower level of detection of 2 to 3 μg g^{-1}/500 μC for thorium and uranium ores. For some ores, however, backgrounds of ~ 20 counts/channel or greater were observed, which reduced the lower level of detection to only 5 to 6 μg g^{-1}/500 μC.

The thorium/uranium Lα peaks are separated by 645 eV; the detector resolution (FWHM) at these X-ray energies is 313 eV. If we assume Gaussian line shapes for both lines, then the peak-to-valley ratio for equal intensity lines should be 9.1:1 and less than 1 per cent of a peak's total area will be folded into its adjacent peak. This is clearly shown to be the case in Figure 3, where the thorium/uranium Lα peaks for concentrations of 75 μg g^{-1} are very well resolved. But the thorium $L\beta_3$ and the uranium $L\beta_1$, whose peaks are separated by only 226 eV (which is less than the peak resolution of 324 eV) as was expected, are not resolved. We have unfolded the thorium Lα peak at the 3σ level for one of our ores with a quoted mixture of 7.8 μg g^{-1} thorium and 4.3 μg g^{-1} uranium but, because of interferences from the adjacent strontium Kα line, the uranium Lα line was only unfolded at the 2σ level. These two points have been plotted in Figures 7 and 8 with reasonable agreement to the fitted lines.

The problem of adjacent peak interferences can be a serious one in

ore analysis. Rubidium and strontium are commonly occurring elements in rock samples and in some ores, and have been observed in concentrations of several hundred $\mu g\ g^{-1}$. The rubidium and strontium Kα lines are within a few hundred eV of the thorium/uranium Lα lines. To compound this problem, the production rates for Kα X-rays in this energy region are 2 to 2.5 times those of Lα X-rays. This can be overcome by using the Lβ or Lγ thorium and uranium peaks and estimating the Lαs from these, knowing the α:β:γ ratios; however, this too can be a problem in the presence of large quantities of yttrium and zirconium.

We have thoroughly investigated the ability of our peak fitting routines to unfold Gaussian peaks interfering in this manner. For Gaussian peaks with heights less than 100:1 and whose separation is greater than their FWHM, the respective peak areas can be unfolded to better than 2 per cent. Non-Gaussian peaks (low energy tailing) are produced by inefficient charge collection in the dead layers at the front face of the detector. This departure from the Gaussian shape becomes apparent at about two FWHM to the low energy side of the peak's centroid (see Figure 6) and the peak-to-tail ratio is about 35:1 at this point. This is much smaller than the peak Gaussian unfolding ratio given above and, more often than not, low energy tailing becomes the dominant factor for small peak unfolding in the presence of a larger, higher energy peak. Small amounts of uranium can be unfolded in larger amounts of thorium much more easily than small amounts of thorium in larger amounts of uranium.

If ore samples contain no rubidium or strontium, spectra having thorium and uranium concentrations that differ by as much as a factor of 50 can be unfolded. If rubidium and/or strontium are present in concentrations greater than 10 to 15 times that of the thorium and/or uranium concentration, then their Lα peaks are obscured and the other L series lines have to be used to obtain a concentration estimate.

Another source of variation is the sample homogeneity and particle size. The PIXE technique is a surface only analysis, the proton range in most samples is only $\sim$ 50 μm and the maximum beam diameter is 2 mm. A simple calculation gives $\sim$ 20 thorium and uranium particles of radius 1 μm in the irradiated volume for 10 $\mu g\ g^{-1}$ in a silicon matrix. For a 5 mm beam diameter, this number would rise to $\sim$ 120. For a fixed concentration, the number of trace element particles is inversely proportional to the cube of their radii. This demonstrates the severe statistical

limitations that particle size and sample homogeneity can produce for small ($\lesssim$ 10 μg g^{-1}) trace element concentrations. For the present experiments, trace element particle sizes were all below 1 μm diameter.

The errors associated with the concentration estimates are themselves a function of the concentration. For concentrations ~ 10 μg g^{-1}, the statistical errors dominate and produce a total relative error of ± 30 per cent. At the 100 μg g^{-1} level, statistics are not so dominant and the total relative error is ± 10 per cent whereas, for concentrations of 1000 μg g^{-1} or greater, experimental errors produced by the total charge reproducibility, *etc.*, dominate and the total relative error is ± 5 per cent. All errors are for the 3σ confidence level.

The technique of a carbon blank background fit for the carbon matrix standards and the ores was very successful and, if 2000 μC runs or greater were used on these blanks to improve the background shape determination, 3σ peak area detection limits of 20 counts, corresponding to 1 to 2 μg g^{-1} per 500 μC or lower, could be obtained. A 2000 μC run on a carbon blank could be done in under an hour of running time before the beginning of a batch of targets.

Further, the use of one Perspex filter instead of four would double the count rate into the thorium and uranium Lα peaks and still attenuate most of the low energy X-ray continuum. Complete removal of the 3 cm air gap between the detector and the base of the target chamber would produce a further factor of 1.5 in the solid angle and hence the count rate into the relevant peak.

When combined, all of these improvements promote confidence in the lower 3σ detection limit of 3 to 4 μg g^{-1} per 100 μC. A 100 μC run at 350 nA takes less than 5 min to complete. The longer 500 μC (24 min at 350 nA) runs were used to increase the accuracy of the lower level limit estimates.

9. THICK TARGET YIELDS

In all experimental work we use thick targets exclusively where the proton range in the matrix (50 μm) is much less than the target thickness (3 mm) and some of the X-rays produced are absorbed by the matrix before reaching the detector. These problems have been studied in detail and the theoretical thick target yields for thorium and uranium L series lines have been calculated.

Figure 9 shows a schematic diagram of a thick target irradiation

depicting the two major processes which result in the reduced X-ray yield as a function of depth:

(i) Proton energy loss due to collisions with matrix atoms, resulting in decreasing X-ray production cross sections as the penetration depth r increases.

(ii) Attenuation of X-rays produced at a depth r in traversing the distance r cot θ through the matrix en route to the detector.

Several authors [Van der Kaan *et al.* 1977; Willis *et al.* 1977; Baeri *et al.* 1978] have considered these problems in detail and several computer codes [Kaufmann *et al.* 1977; Van Espen *et al.* 1977; Willis & Walter 1977] have been written to enable them to be solved. Following Willis *et al.* [1977] for the total thick target L X-ray yield

$$N^L = \frac{CN_o}{W} \frac{\Omega It\varepsilon}{4\pi e} \int_{E_p}^{o} \sigma_x^L \frac{dE}{S(E)} \exp -\mu \int_{E_p}^{E} \frac{dE}{S(E)} \cot\theta \ , \qquad (9)$$

where $\sigma_x^L = \sigma_I \bar{\omega}_L$; is the X-ray production cross section for all L transitions (cm^2),

$\mu = \Sigma \mu_j c_j$; is the composite matrix mass attenuation coefficient ($cm^2\ g^{-1}$),

$S(E) = \Sigma \delta_j c_j$; is the composite proton stopping powers of the matrix (MeV $cm^2\ g^{-1}$),

σ_I = the proton ionisation production cross section for the trace element being considered,

$\bar{\omega}_L$ = the mean fluorescence yield for all the L transitions,

μ_j = mass attenuation coefficient of the j^{th} matrix element,

S_j = proton stopping power of the j^{th} matrix element,

c_j = the relative concentration by weight of the j^{th} matrix element,

C = the relative concentration by weight of the trace element being considered,

N_0 = Avogadro's number,

W = the atomic weight of the trace element (g),

Ω = the solid angle subtended by the detector (steradian),

It = the total proton charge impinging on the target (coulomb),

ε = the detector efficiency including all absorptive materials between the detector and the target,

Ξ Eff% as defined by Equation (1) in the present case,

e = electronic charge (coulomb),

E_p = initial proton energy (2.26 MeV), and
θ = target angle (45°).

This equation has been used to calculate the total L X-ray yields for a carbon matrix and two ore matrices, GSP-1 and SY-2 [Flanagan 1973], for the Z range 72 to 95, a proton energy of 2.26 MeV and a target angle of 45°. The results are shown in Figure 10 for the number of counts per 100 μg g^{-1} per 100 μC and a solid angle of 2.2 x 10^{-3} steradians. For comparison, the yields for E_p = 3 MeV and a carbon matrix are shown. An increase in the initial proton energy to 3 MeV would produce a factor of 3.4 in the total L X-ray production rate. For very low level concentrations of thorium and uranium, however, this increase could be offset by a corresponding tenfold increase in the γ-ray induced background [Bauer & Gippner 1978] and a subsequent loss of sensitivity. Figure 10 also indicates a 12 per cent decrease in the thorium/uranium L X-ray yield for the carbon matrix compared with the ore matrix. This difference is clearly seen in Figures 7 and 8 where the least squares fits to experimental results have been plotted. The thorium Lα carbon-to-ore matrix results differ by ~ 10 per cent and the uranium Lα results by ~ 9 per cent. This is in reasonable agreement with our calculated value of ~ 12 per cent.

The mass attenuation coefficients and stopping powers required to produce these curves were taken from the tables of Theisen & Vollath [1967] and Williamson *et al.* [1966], respectively, and the ionisation production cross sections were calculated using the polynomial fits of Johansson & Johansson [1976] and the fluorescence yields from the tables of Bambynek *et al.* [1972]. As far as can be estimated, these would produce a total error in the total L X-ray count of between 5 and 15 per cent.

The bulk compositions of the USGS-GSP-1 granodiorite and the SY-2 Canadian reference rock standards are given in Table 2. The trace element concentrations for most elements are also known [Flanagan 1973; Abbey *et al.* 1975], but not listed here. The thorium/uranium concentrations for GSP-1 are 104 and 2 μg g^{-1} respectively and, for SY-2 370 and 290 μg g^{-1} respectively.

The curves of Figure 10 enable a calculated value for the total number of L X-rays produced in an ore or carbon matrix to be obtained for any trace element from Ta to Am. More particularly, using the measured α:β:γ ratios for thorium and uranium given in Table 1, the

number of Lα X-ray counts per 100 μg g^{-1} per 100 μC can be estimated. Table 3 gives a comparison between calculated and experimental values; the experimental yields are seen to be in excellent agreement with calculated thick target yields for both carbon and ore matrices.

The GSP-1 and SY-2 ores used did not differ significantly from the rest of the ores; their equivalent atomic numbers (Z) by weight were 11.9 and 10.7 respectively. The thick target yields for thorium and uranium in pure matrices with $6 < Z < 30$ are shown in Table 4. These yields do not differ significantly with Z until the energy of the K edge of the matrix approaches the Lα energy of the trace element X-ray. The thorium and uranium Lα yields are effectively constant over the equivalent Z range of most common ores.

10. SUMMARY

Using the PIXE technique, concentrations of thorium and uranium have been measured simultaneously in a variety of ore matrices. The minimum available trace element concentration in an ore was 7.8 μg g^{-1} of thorium, together with 4.3 μg g^{-1} of uranium. These were measured with a total relative error at the 3σ level of ± 30 per cent. For the majority of ores containing concentrations of 1000 μg g^{-1}, the total errors are only ± 5 per cent.

The lower level detection limit, with no adjacent element interferences is 3 to 4 μg g^{-1} per 100 μC if the background component is ~ 5 counts per channel and the proton energy is 2.26 MeV. For ores containing large amounts of sodium and aluminium, the γ-ray induced background in the X-ray region of interest can be higher than 20 counts per channel. This will raise the lower level detection limit to 7 or 8 μg g^{-1} per 100 μC or greater.

In the absence of rubidium and strontium, the thorium and uranium Lα lines are clearly resolved and spectra produced by thorium and uranium, whose concentrations differ by as much as a factor of 50, can still be unfolded. The low energy tail present on all peaks indicates that small amounts of uranium can be analysed in larger amounts of thorium much more accurately than small amounts of thorium in larger amounts of uranium.

The spectrum fitting routines can unfold the Kα series peaks interfering with the Lα peaks, provided that the low atomic number trace element concentrations do not exceed the corresponding thorium/uranium

concentrations by a factor of 10 to 15. If the thorium/uranium Lα peaks are completely obscured by the rubidium and strontium Kα peaks, then the thorium/uranium $L\beta_1$ or $L\beta_3$ peaks can be used, and their known ratios to the Lα peak provide an estimate for the Lα peak area. In such a case, since Lβ peaks are 2 to 3 times smaller than the Lα peak, only concentrations of yttrium and zirconium less than 3 to 5 times that of the thorium/uranium concentrations can be tolerated.

The complete thick target calculations have been made for a carbon matric and two ore matrices whose bulk compositions were known. Differences in the Lα X-ray yields for the two types of matrices were very well predicted by the theory and these differences, although only ~ 10 per cent, were observed experimentally.

A system for thick target thorium and uranium analysis which meets geologists' exploration needs is now available. Irradiation times are short and up to 12 samples an hour can be processed. Simple spectra can be analysed immediately in real time on the PDP15 computer used to collect the data. More complicated spectra can be transferred to a larger computer for background fitting and peak unfolding analysis. These are done as batch jobs, taking typically 10 min of CPU time to process more than 20 spectra.

The PIXE technique has been used for the absolute determination of thorium and uranium concentrations, but obviously it could be extended to other elements in a similar X-ray energy region.

11. ACKNOWLEDGEMENTS

The authors thank H. Broe, J.P. Fallon, L.H. Russell and M.J. Kenny for their assistance with the accelerator and installation of the target chamber and its ancillary equipment. M.D. Scott and R.J. Cawley assembled and programmed the software for data acquisition; Mr Scott also designed and built the carbon filament and battery needed to overcome the high target potential problem. This research was partly funded by the Australian Institute of Nuclear Science and Engineering.

12. REFERENCES

Abbey, S., Gillieson, A.H. & Perrault, G. [1975] - CANMET MSL Technical Report.

Baeri, P., Campisano, S.U., Immé, G., Rimini, E. & Della Mea, G. [1978] - *Nucl. Instrum. Methods*, 149 : 435.

Bambynek, W., Crasemann, B., Fink, R.W., Freund, H.-U., Mark, H., Swift, C.D., Price, R.E. & Venugopala Rao, P. [1972] - *Rev. Mod. Phys.*, 44 : 716.

Bauer, C. & Gippner, P. [1978] - *Z. Phys.*, A284 : 275.

Bearse, R.C., Close, D.A., Malanify, J.J. & Umbarger, C.J. [1974] - *Anal. Chem.*, 46 : 499.

Beech, A.M. & Eberhardt, J.E. [1973] - AAEC/E297.

Cohen, D.D. & Duerden, P. [1979] - AAEC/E453.

Clayton, E., Cohen, D.D. & Duerden, P. - AAEC report forthcoming.

Deconninck, G. [1977] - *Nucl. Instrum. Methods*, 142 : 275.

Deconninck, G., Demortier, G. & Bodart, F. [1975] - *At. Energy Rev.*, 13 : 367.

D'Silva, A.P. & Fassel V.A. [1977] - *Anal. Chem.*, 49 : 638.

Flanagan, F.J. [1973] - *Geochim. Cosmochim. Acta*, 37 : 1189.

Folkmann, F., Gaarde, C., Huus, T. & Kemp, K. [1974] - *Nucl. Instrum. Methods*, 116 : 487.

Garner, E.L., Machlan, L.A. & Shields, W.P. [1971] - US National Bureau of Standards Special Publ., 260 : 27, 162.

Giauque, R.B., Garrett, R.B. & Goda, L.Y. [1977] - *Anal. Chem.*, 49 : 1012.

Guffey, J.A., van Rinsvelt, H.A., Sarper, R.M., Karcioglu, Z., Adams, W.R. & Fink, R.W. [1978] - *Nucl. Instrum. Methods*, 149 : 489.

Johansson, S.A.E. & Johansson, T.B. [1976] - *Nucl. Instrum. Methods*, 137 : 473.

Kaji, H., Shiokawa, T., Ishii, K., Morita, S., Kamiya, M., Sera, K. & Tawara, H. [1977] - *Nucl. Instrum. Methods*, 142 : 21.

Kaufmann, H.C., Akselsson, K.R. & Courtney, W.J. [1977] - *Nucl. Instrum. Methods*, 142 : 251.

Keenan, J.A. [1975] - *Appl. Spectrosc.*, 29 : 63.

Mahajan, G.R., Chaudhuri, N.K., Sampathkumar, R. & Iyer, R.H. [1978] - *Nucl. Instrum. Methods*, 153 : 253.

Mittler, A., Barnes, B.K., Litman, R., Holton, F. & Barry, E.F. [1977] - *Anal. Chem.*, 49 : 432.

Nielson, K.K., Hill, M.W., Mangelson, N.F. & Nelson, F.W. [1976] - *Anal. Chem.*, 48 : 1947.

Ragaini, R.C., Heft, R.E. & Garvis, D. [1976] - UCRL-52092.

Raith, B., Roth, M., Göllner, K., Gonsior, B., Osterman, H. & Uhlhorn, C.D. [1977] - *Nucl. Instrum. Methods*, 142 : 39.

Simpson, A.E. & Dyson, N.A. [1977] - *Nucl. Instrum. Methods*, 146 : 473.

Theisen, R. & Vollath, D. [1967] - Tables of X-ray Mass Attenuation Coefficients. Verlag Stahleisen GMbH, Düsseldorf.

Van der Kam, P.M.A., Vis, R.D. & Verheul, H. [1977] - *Nucl. Instrum. Methods*, 142 : 55.

Van Espen, P., Nullens, H. & Adams, F. [1977] - *Nucl. Instrum. Methods*, 142 : 243.

Wall, T. [1978] - 2nd Aust. Conf. on Nuclear Techniques of Analysis. Australian Institute of Nuclear Science & Engineering, Lucas Heights, p.118.

Walter, R.L., Willis, R.D., Gutknecht, W.F. & Joyce, J.M. [1974] - *Anal. Chem.*, 46 : 843.

Williamson, C.F., Boujot, J. & Picard, J. [1966] - CEA-R3042.

Willis, R.D. & Walter, R.L. [1977] - *Nucl. Instrum. Methods*, 142 : 231.

Willis, R.D., Walter, R.L., Shaw, R.W. & Gutknecht, W.F. [1977] - *Nucl. Instrum. Methods*, 142 : 67.

TABLE 1

MEASURED THORIUM AND URANIUM $\alpha:\beta:\gamma:\ell:\eta$ RATIOS FOR OUR DETECTION SYSTEM USING FOUR LAYERS OF PERSPEX FILTERS

Z	Elt.	Relative Intensities						
		$L\ell$	$L\alpha$	$L\eta$	$L\beta_1$	$L\beta_2$	$L\gamma_1$	$L\gamma_2$
90	Th	0.037	1.000	0.022	0.504	0.367	0.104	0.030
92	U	0.039	1.000	0.021	0.408	0.345	0.095	0.027

TABLE 2

RECOMMENDED VALUES FOR THE MAJOR CONSTITUENTS OF THE KNOWN ORE SAMPLES GSP-1 AND SY-2

Compound	Concentration % by weight	
	GSP-1	SY-2
SiO_2	67.4	60.1
Al_2O_3	15.3	12.2
Fe_2O_3	1.8	2.3
FeO	2.3	3.6
MgO	1.0	2.7
CaO	2.0	8.0
Na_2O	2.8	4.4
K_2O	5.5	4.5
TiO_2	0.66	0.15
P_2O_5	0.28	0.44

TABLE 3

COMPARISON OF THEORETICAL AND EXPERIMENTAL Lα X-RAY COUNTS PER 100 μg g^{-1} PER 100 μC FOR E_p = 2.26 MeV, Ω = 2.2 x 10^{-3} sr FOR A CARBON AND ORE MATRIX USING FOUR LAYERS OF PERSPEX FILTERS

Matrix	Lα counts/100 μg g^{-1}/100 μC			
	Calculated		Experimental	
	Th	U	Th	U
Carbon	280±25	263±24	296±20	258±20
Ore SY-2	320±32	302±30	328±30	284±25
Ore GSP-1	320±32	302±30		

TABLE 4

Lα X-RAY COUNTS FOR VARIOUS MATRICES

Element	Atomic No.	Calculated Lα Counts per 100 μg g^{-1} per 100 μC	
		Th	U
C	6	280±28	263±26
Na	11	328±33	310±31
Si	14	337±34	319±32
Ca	20	343±34	328±33
Fe	26	330±33	324±32
Cu	29	310±31	308±31

E_p = 2.26 MeV; Ω = 2.2 x 10^{-3} steradians

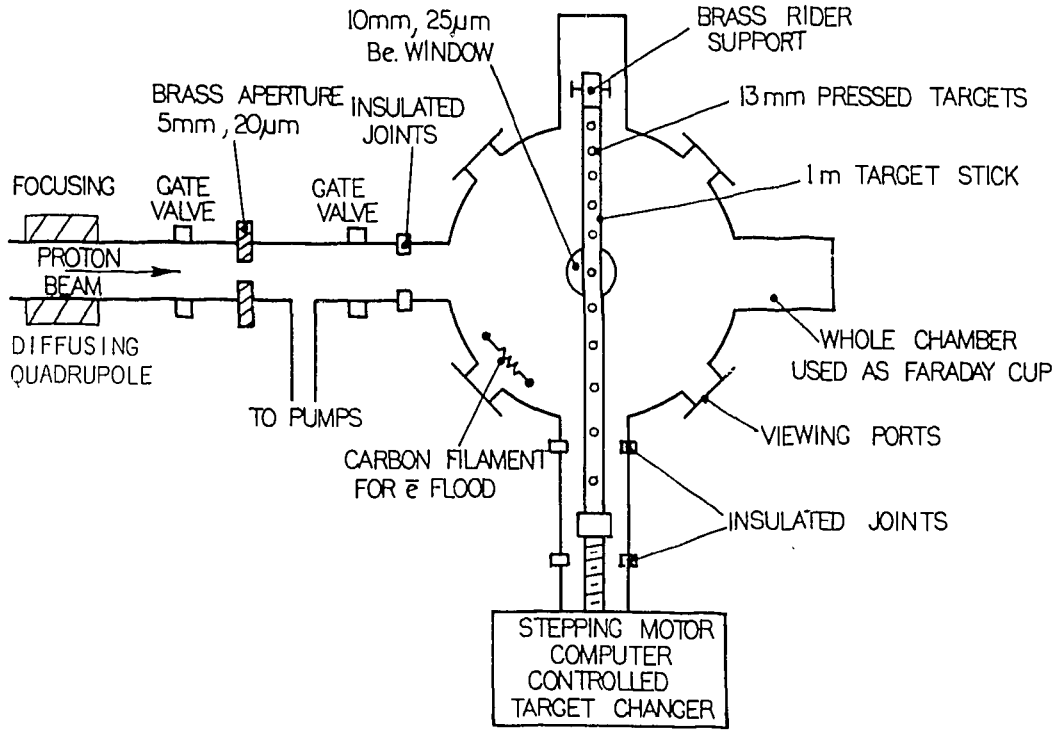

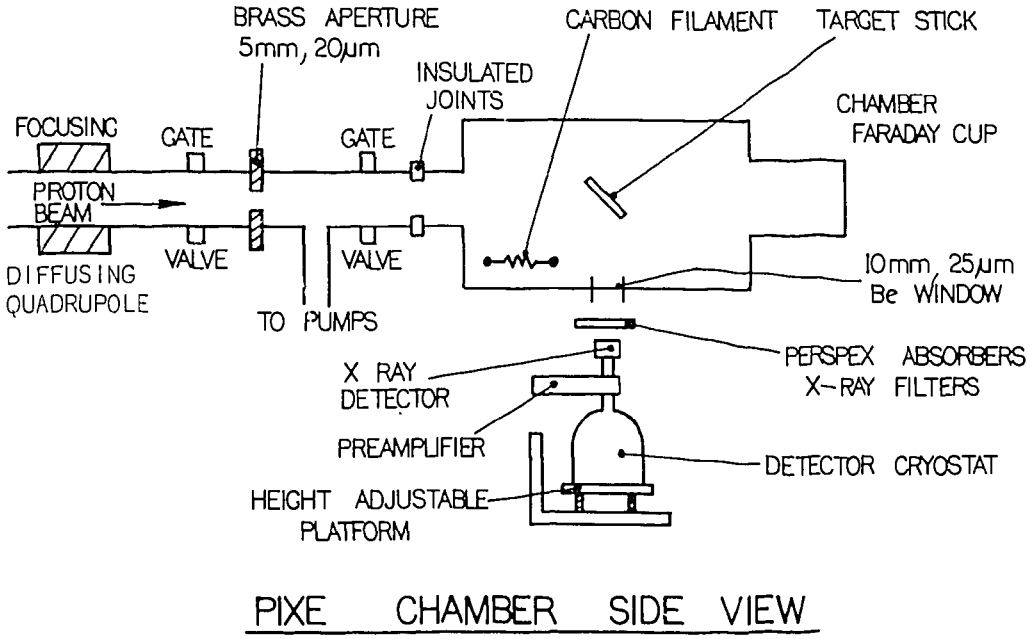

FIGURE 1. SCHEMATIC DIAGRAM OF THE EXPERIMENTAL ARRANGEMENT

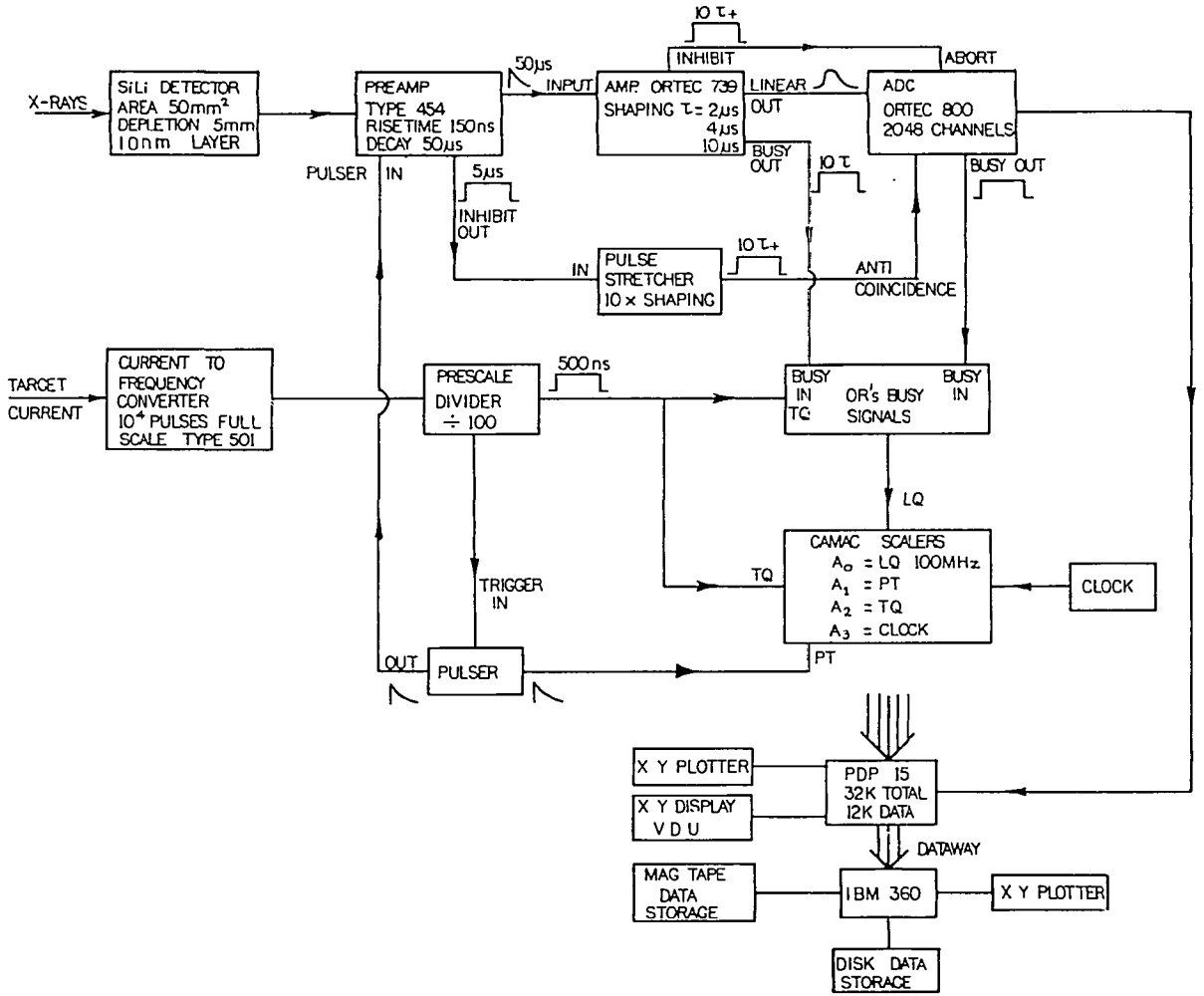

FIGURE 2. SCHEMATIC DIAGRAM OF THE ELECTRONICS SYSTEM

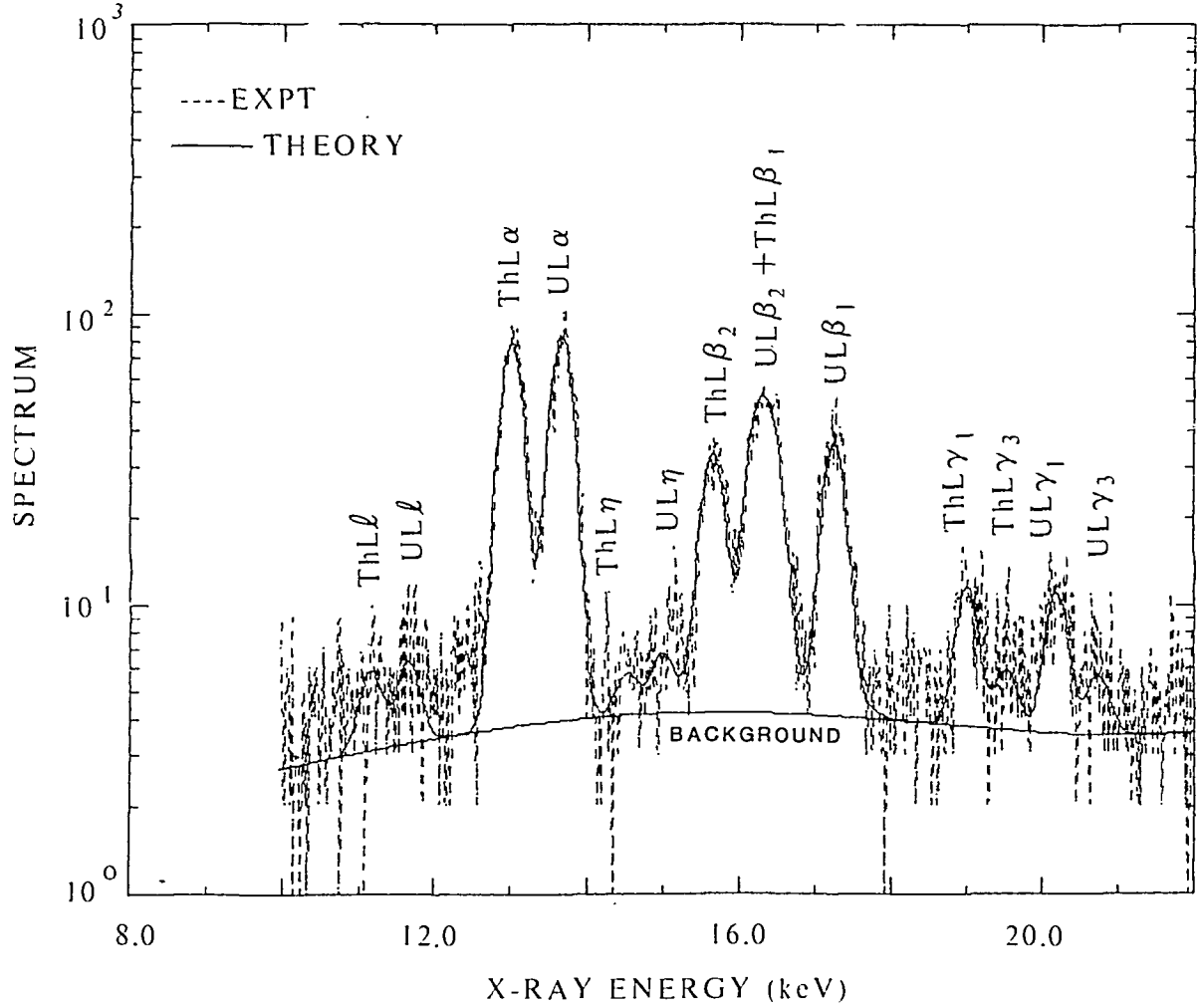

FIGURE 3. TYPICAL PIXE SPECTRA FOR 75 μg g^{-1} THORIUM AND URANIUM IN A CARBON MATRIX

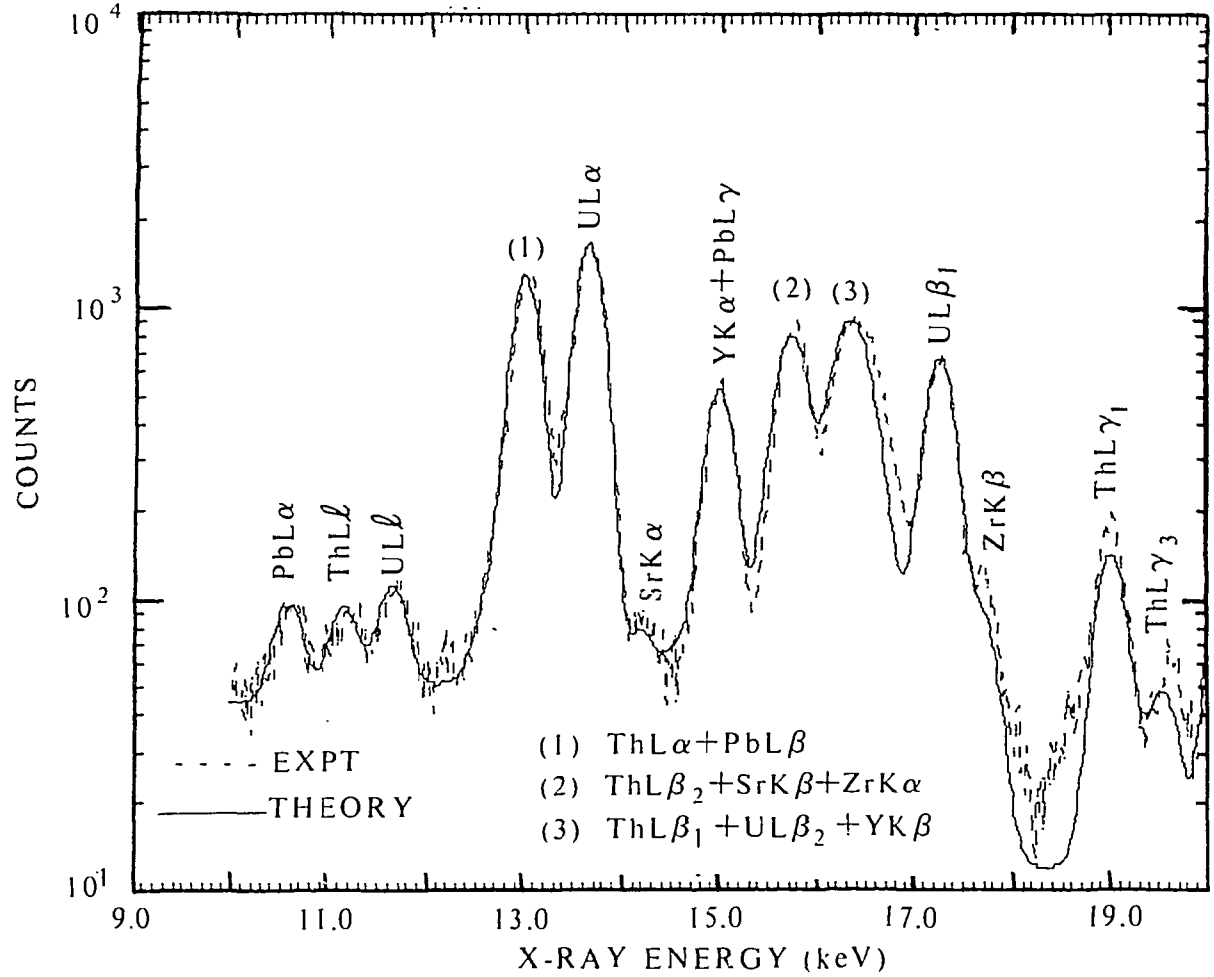

FIGURE 4. TYPICAL PIXE SPECTRA FOR 1043 μg g^{-1} THORIUM, 1740 μg g^{-1} URANIUM IN AN ORE MATRIX

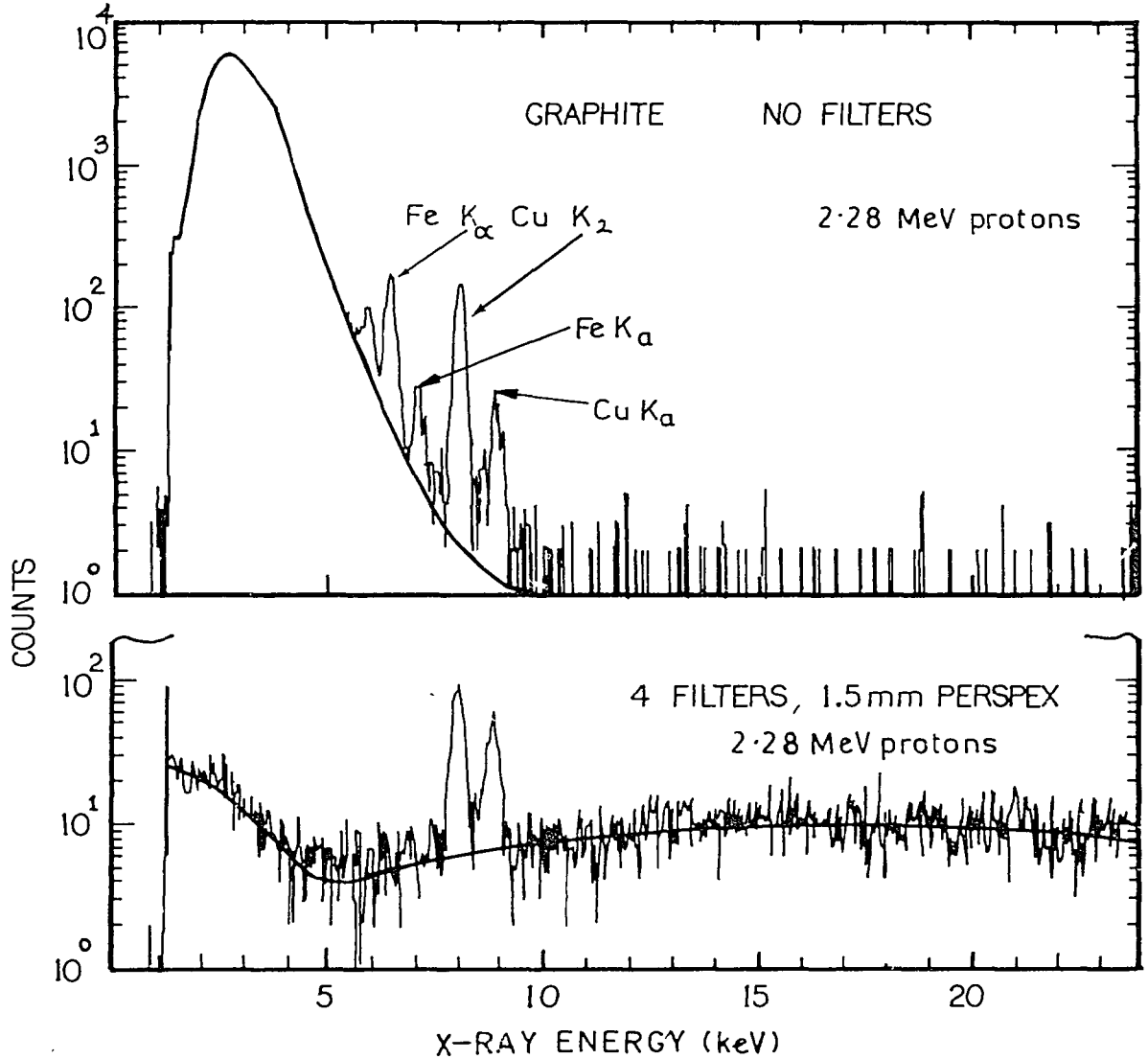

FIGURE 5. BACKGROUND RADIATION FROM A CARBON MATRIX WITH/WITHOUT FILTERS

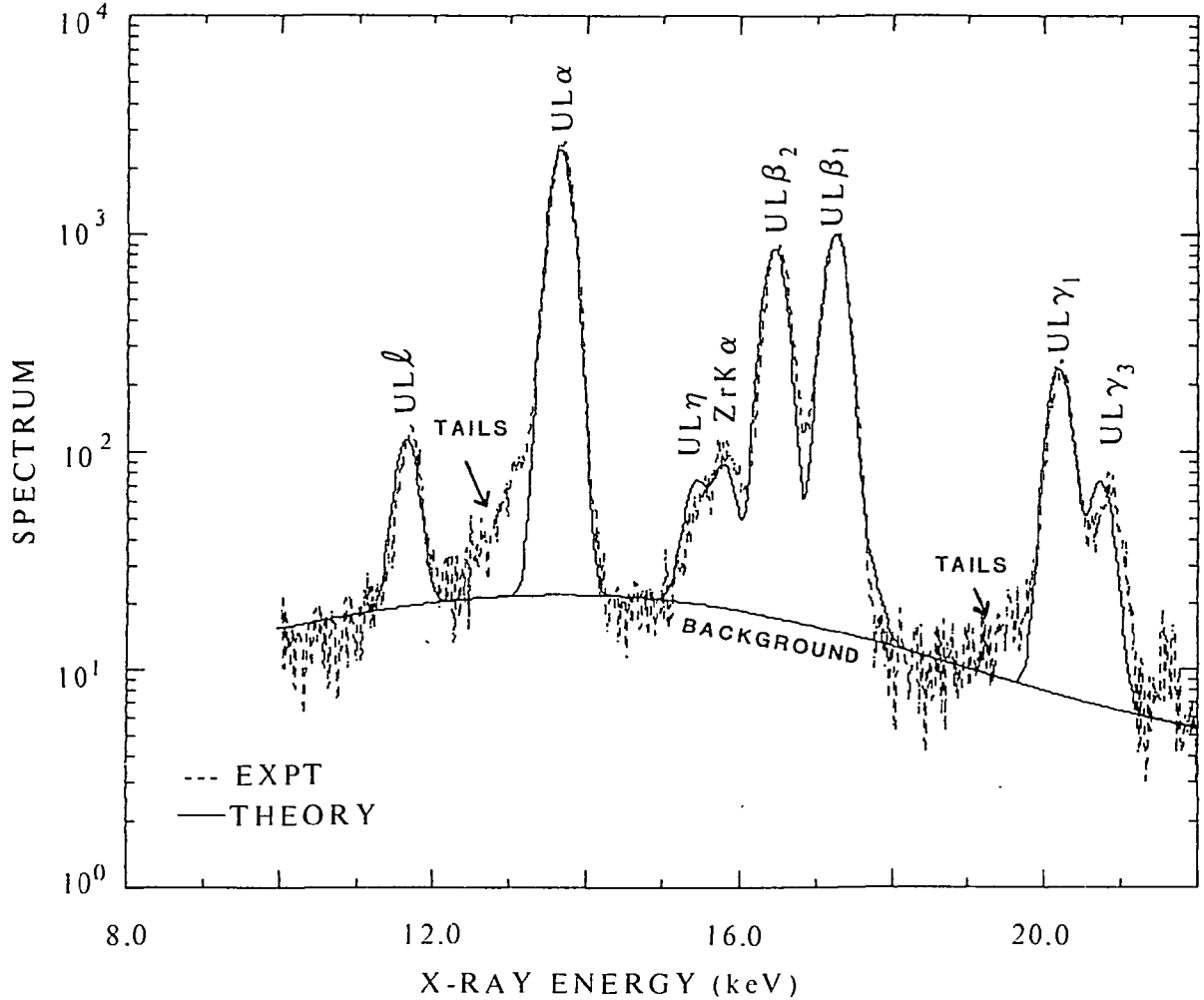

FIGURE 6. PIXE SPECTRA FOR 3584 μg g^{-1} URANIUM IN A CARBON MATRIX, SHOWING LOW ENERGY TAILING

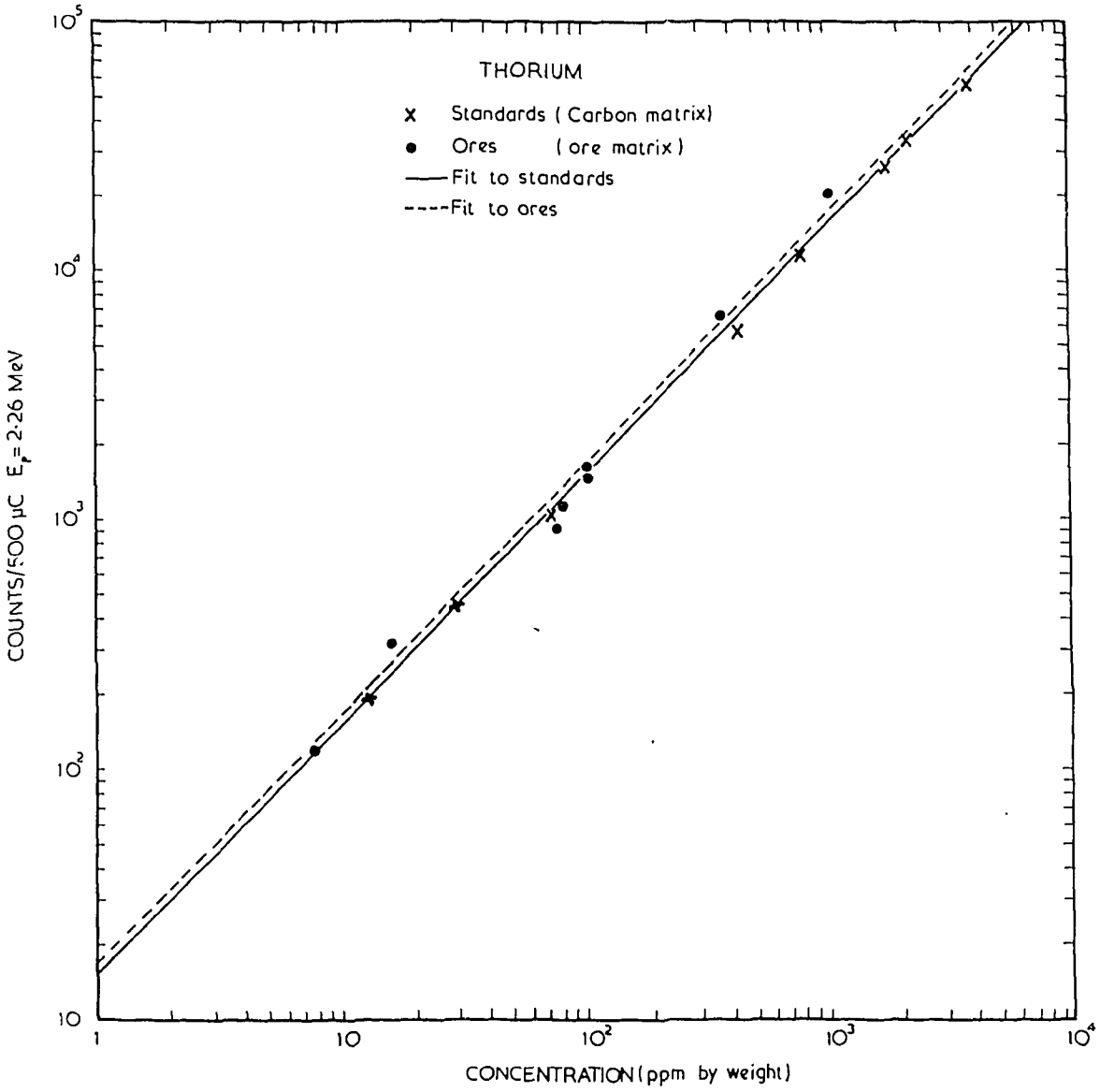

FIGURE 7. THORIUM Lα PEAK AREA VERSUS CONCENTRATION

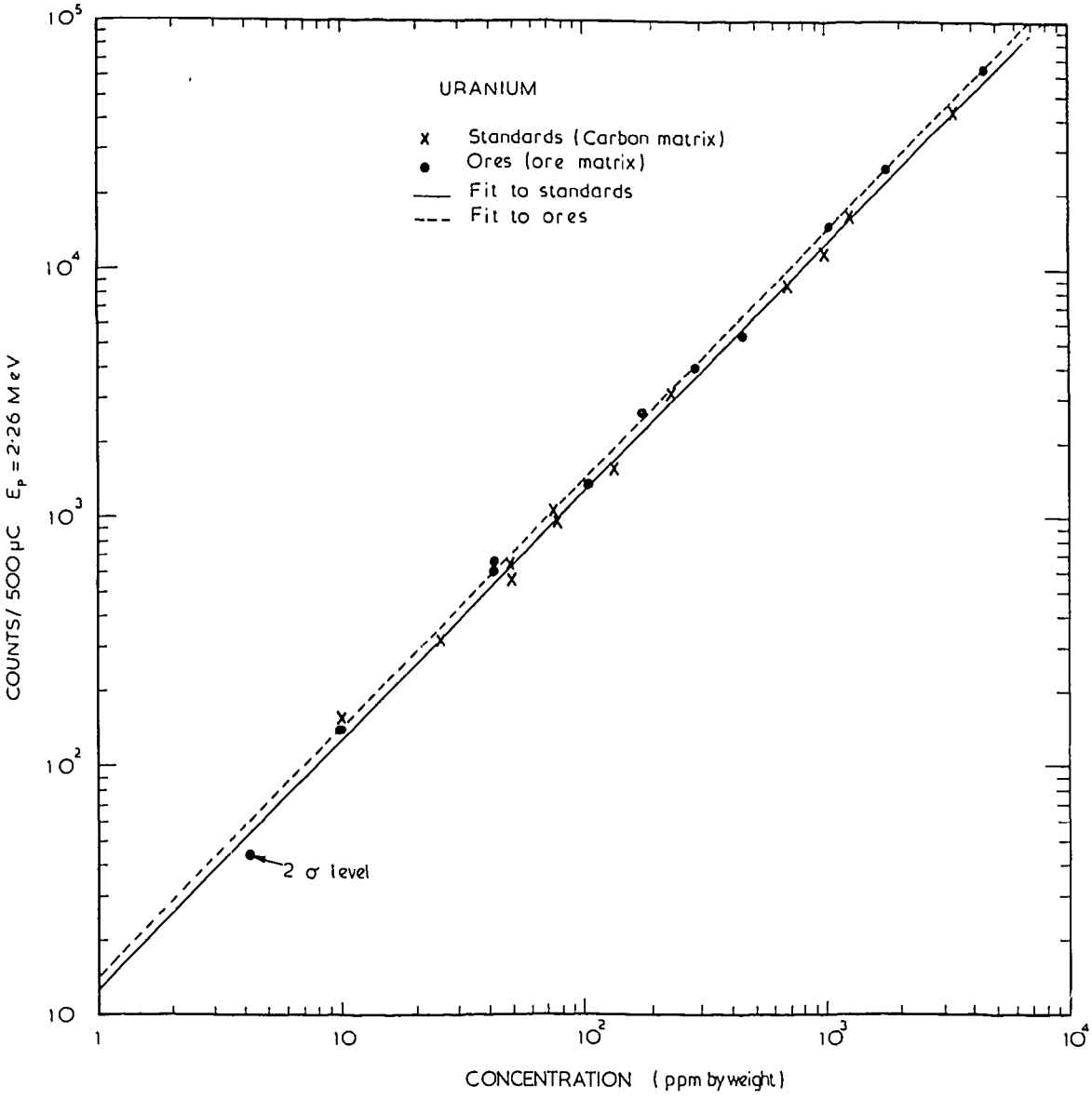

FIGURE 8. URANIUM Lα PEAK AREA VERSUS CONCENTRATION

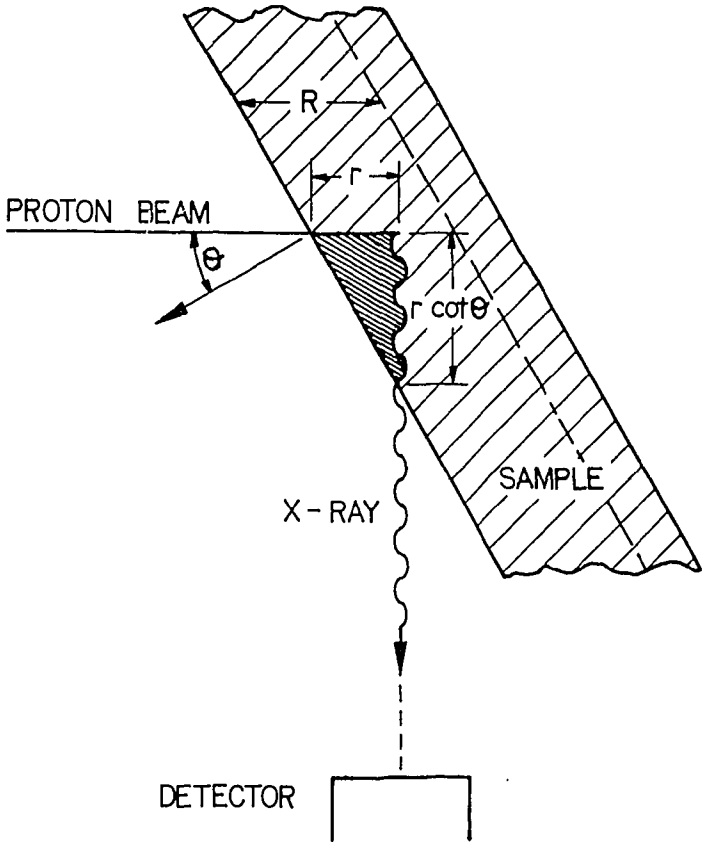

R - RANGE OF PROTONS IN SAMPLE
r - ARBITRARY PENETRATION DEPTH
AT WHICH X-RAY IS PRODUCED
θ - ANGLE OF INCLINATION OF SAMPLE

FIGURE 9. SCHEMATIC OF A THICK TARGET IRRADIATION

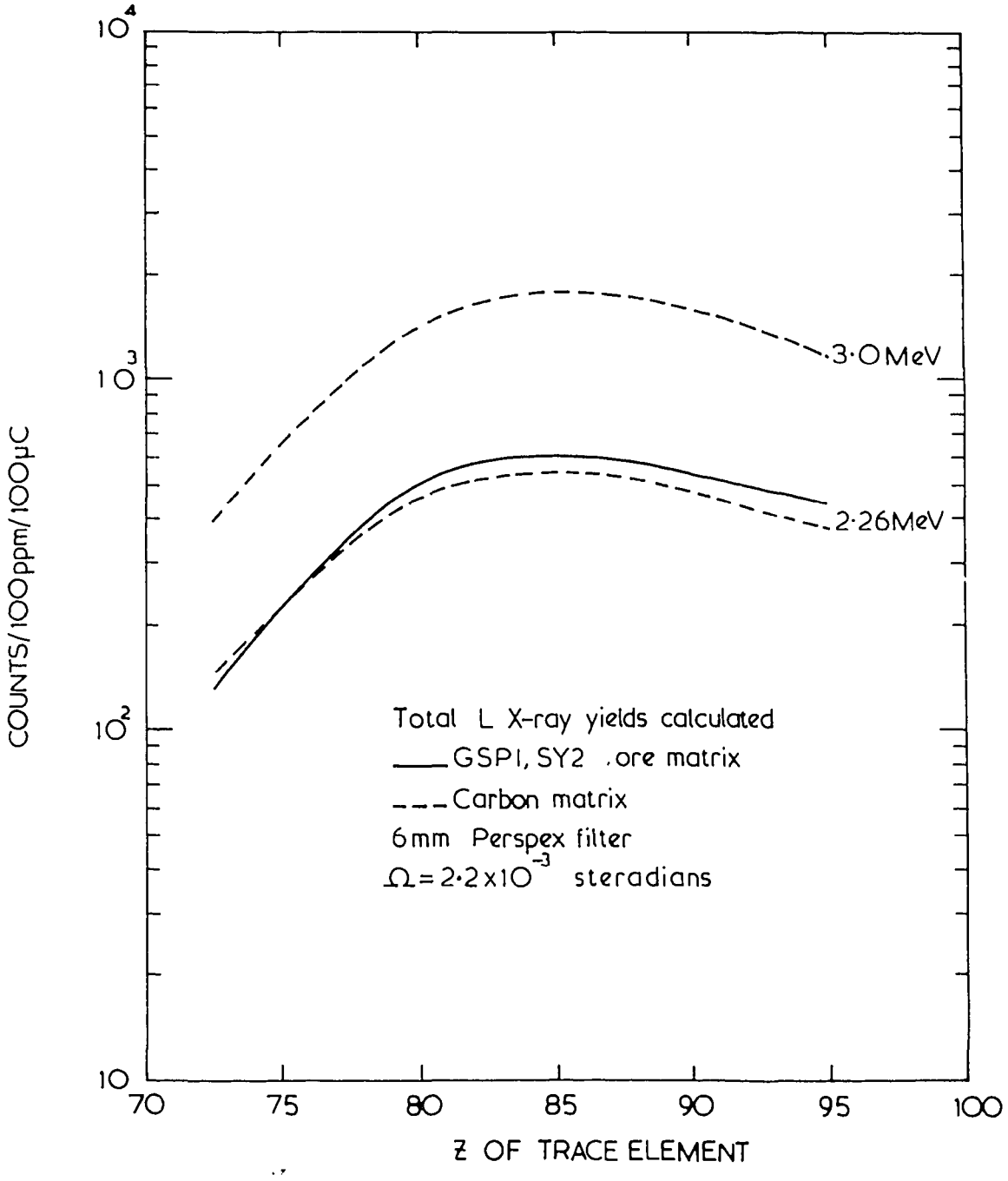

FIGURE 10. CALCULATED TOTAL L X-RAY YIELDS VERSUS Z OF THE TRACE ELEMENT

Printed by the AAEC Research Establishment